

Implications of RNA Structure on the Annealing of a Potent Antisense RNA Directed against the Human Immunodeficiency Virus Type 1[†]

Sigrid Eckardt,[‡] Pascale Romby,[§] and Georg Sczakiel^{*,‡}

Forschungsschwerpunkt Angewandte Tumorstudiologie, Deutsches Krebsforschungszentrum, Im Neuenheimer Feld 242, D-69120 Heidelberg, Germany, and Institut de Biologie Moléculaire et Cellulaire de CNRS, 15 rue René Descartes, 67084 Strasbourg Cedex, France

Received March 27, 1997; Revised Manuscript Received July 21, 1997[®]

ABSTRACT: Antisense RNA-mediated regulation in bacterial systems is related to the kinetics of RNA–RNA annealing *in vitro*. Here, we investigated the secondary structure of α Y69, an effective HIV-directed antisense RNA in human cells. Purified RNA preparations contain a single conformer. The global structure was identified by a cleavage experiment under native conditions using a short complementary oligonucleotide and RNase H. Structural analyses indicate a three-domain structure of α Y69 consisting of two stem–loop elements connected by a seven-nucleotide single-stranded hinge region. Kinetic data suggest that the formation of base pairs between a CGC triplet of α Y69 and its target RNA is essential for fast annealing. The complementary sequence stretch of the target folds into a high-energy secondary structure. The relationship between modifications in structural elements of α Y69 and the annealing kinetics suggested that rate-limiting steps of the annealing involve a single site of α Y69 and do not involve its 5' or 3'-end. Further, the data indicate that both initial base-specific interactions and duplex formation are dependent on the CGC triplet of the central region of α Y69. This mechanism represents a specific and efficient way of RNA–RNA annealing that is initiated by the interaction of unstructured RNA regions.

Antisense RNA-mediated control of gene expression and plasmid replication is an efficient regulatory mechanism originally discovered in bacteria (Wagner & Simons, 1994; Simons & Kleckner, 1988). Artificial antisense RNA is receiving increased attention as an inhibitor of aberrant gene expression and viral functions in eukaryotic cells (Erickson & Izant, 1992). The present understanding of the mechanisms of antisense inhibition is largely derived from the detailed studies on naturally occurring bacterial systems, e.g. the control of ColE1 and R1 plasmid copy number in *Escherichia coli* (Eguchi & Tomizawa, 1991; Wagner & Simons, 1994). Fast binding of the complementary RNA *in vitro* is correlated with the inhibitory efficacy *in vivo* indicating that a mechanism allowing fast RNA–RNA annealing is crucial for antisense inhibition. In the ColE1 system, an initial intermolecular interaction between three complementary stem–loop structures of sense and antisense RNA leads to the formation of a reversible complex termed the kissing complex (Eguchi *et al.*, 1991; Eguchi & Tomizawa, 1990, 1991). Subsequently, duplex formation is initiated by base pairing between the free 3'-end of the antisense RNA and an unpaired region within the target RNA (Eguchi *et al.*, 1991). A kissing complex between complementary stem–loop elements also constitutes the rate-limiting interaction between copA and copT RNA involved in regulation of R1 plasmid copy number (Wagner & Simons, 1994; Persson *et al.*, 1990). Interestingly, initial recognition

via the reversible complex and the following initiation and elongation of duplex formation do not occur at the same site. These “two-site” pathways of RNA duplex formation represent fast binding mechanisms with association rate constants on the order of $10^6 \text{ M}^{-1} \text{ s}^{-1}$. Conversely, a mechanism involving only a single critical site has been proposed for the interaction of RNA-IN and RNA-OUT in the regulation of transposon TN10.¹ The initial interaction between a stem–loop element of the antisense RNA-OUT and the unstructured 5'-end of RNA-IN proceeds to the initiation of complete duplex formation within the same site (Kittle *et al.*, 1989). A “single-site” binding pathway that involves an unpaired 5'-end has also been reported for the *hok-sok* system of *E. coli* (Thisted *et al.*, 1994).

In all antisense RNA-regulated systems analyzed so far, mutations that reduce the association rate of the complementary RNA *in vitro* result in loss of inhibitory efficacy *in vivo* (Wagner & Simons, 1994; Hjalt & Wagner, 1992; Jain, 1995; Case *et al.*, 1989). The correlation between efficient antisense inhibition and fast association kinetics, however, is directly related to the structures of the RNA involved. For artificial antisense RNA directed against HIV-1, a similar correlation between RNA–RNA annealing kinetics *in vitro* and efficacy in human cells has been observed (Rittner *et al.*, 1993). The HIV-1 *tat/rev*-directed antisense RNA α Y69 is a very strong antisense inhibitor of HIV-1 replication in human cells (Homann *et al.*, 1993; Junker *et al.*, 1994). Predicted secondary structure models and preliminary mutational analysis showed that α Y69 is structurally different

[†] S.E. was supported by the Deutsche Forschungsgemeinschaft (Grant Sc14-1/2).

* Corresponding author. Telephone: +49 6221-424939. Fax: +49 6221-424932. E-mail: Sczakiel@dkfz-heidelberg.de

[‡] Deutsches Krebsforschungszentrum.

[§] Institut de Biologie Moléculaire et Cellulaire de CNRS.

[®] Abstract published in *Advance ACS Abstracts*, September 1, 1997.

¹ Abbreviations: CMCT, 1-cyclohexyl-3-(2-morpholinoethyl)carbodiimidemetho-*p*-toluenesulfonate; DMS, dimethyl sulfate; HIV-1, human immunodeficiency virus type 1; kethoxal, β -ethoxy- α -ketobutyraldehyde; TN10, transposon 10.

from natural antisense RNA and is not compatible with the known annealing mechanisms from prokaryotic systems. The high efficacy of α Y69 in living cells [$> 99\%$ inhibition; see ref. Homann *et al.* (1993)] suggests that the underlying mechanism represents an effective alternative to most of the natural antisense-regulated systems studied so far.

In this work, we present data from a detailed structural analysis that provide conclusive evidence that *in vitro* the antisense RNA α Y69 exists in a specific structure of two stem-loop helices that are linked by a seven nucleotide hinge region. By using truncated or modified derivatives of α Y69, we relate the association kinetics between α Y69 and the complementary sense RNA SR6 (645 nucleotides) to the structural model for α Y69. The data of this work suggest that interactions between a base triplet located within a flexible region of the antisense RNA α Y69 and a high-energy region of its target RNA are rate-limiting for annealing.

MATERIALS AND METHODS

Computer Programs. Secondary structures were calculated using the program mfold, versions 2.0 and 2.3. The minimal folding potential for SR6 was determined with the program foldsplit (Sczakiel *et al.*, 1993) with a window of 100 nucleotides and a step width of 1 nucleotide. Both programs are based on the GCG package (Devereux *et al.*, 1984) and are available from the computer service HUSAR [Heidelberg Unix Sequence Analysis Resources (Senger *et al.*, 1995)].

Preparation of RNA. The RNA α Y69 was prepared by run-off transcription *in vitro* with T7 RNA polymerase from the *Bg*/II-linearized plasmid p α Y69 containing the T7 promoter-driven transcription cassette for α Y69 (Homann *et al.*, 1993). The α Y69 mutants α Y69-1–5 contain three base exchanges at positions 26–28 and were transcribed from double-stranded oligodeoxyribonucleotides containing the T7 promoter sequence and the respective base exchanges. The sense RNA SR6 (Rittner & Sczakiel, 1991; Rittner *et al.*, 1993) and SR6-5 were transcribed *in vitro* from the plasmids pSR6 and pSR6-5, respectively, linearized with *Not*I. The plasmid pSR6-5 was generated by site-directed mutagenesis of pSR6 introducing three base exchanges at positions 278–280 of SR6 (QuikChange Site-Directed Mutagenesis Kit, Stratagene). *In vitro* transcription, purification, and end labeling of RNA were performed as described by Kronenwett *et al.* (1996). Under the experimental conditions, purified RNA preparations contained only the double-rod conformer of α Y69.

The oligoribonucleotide α Y30 (positions 1–30 of α Y69) was purchased from a commercial supplier. The oligoribonucleotides asl-1 (22 nucleotides, positions 14–35 of α Y69) and α Y9_{mod} (36 nucleotides, 5'-AGCCUUAAG-GCUCGUCGUCGAGCAGAGACUGCUUC-3'; underlined bases are complementary to SR6) were chemically synthesized and kindly provided by M. Sprinzl (University of Bayreuth). 5'-End labeling and purification were performed as described above.

Renaturation of RNA was carried out either by 10 min of incubation of the RNA at 70 °C and subsequent slow cooling to 20 °C or by 2 min of incubation at 90 °C, quick chilling on ice, and a prolonged incubation at 20 °C in the respective buffer for enzymatic or chemical modification. Chemical and RNase V1 reaction mixtures were supplemented with 1 μ g of total tRNA.

Probing of RNA with Oligodeoxyribonucleotides and RNase H. A 7mer oligodeoxyribonucleotide complementary to positions 24–30 of α Y69 was annealed to either 5'-end- or uniformly labeled α Y69 or to 5'-end-labeled asl-1 RNA in hybridization buffer containing 100 mM NaCl, 10 mM MgCl₂, and 20 mM Tris/HCl at pH 7.6 for 30 min at 37 °C (10 μ M final concentration of oligodeoxyribonucleotide). Reaction mixtures were cooled to room temperature for 20 min prior to addition of 1 unit of RNase H (Boehringer, Mannheim, Germany). After 15 min, reaction mixtures were placed on ice and further analyzed (i) by denaturing polyacrylamide gel electrophoresis (12% polyacrylamide, 8 M urea; samples heated in 95% formamide and dyes to 95 °C for 3 min prior to electrophoresis) to verify the cleavage product size and the position of the label and (ii) by nondenaturing polyacrylamide gel electrophoresis in a sample buffer containing 10 mM Tris/HCl (pH 7.6), 1 mM EDTA, 0.1% SDS, 6% sucrose, 0.25% bromophenol blue, and 0.25% xylene cyanol on horizontal 10% polyacrylamide gels (0.1 \times TBE, no urea) placed on a uniformly cooled (12 °C) metal block (Qiagen TGGE System, Qiagen, Hilden, Germany). For analysis of asl-1 RNase H cleavage products by RNase T1, aliquots of the reaction mixture were incubated in hybridization buffer at room temperature or at 95 °C for 3 min. After quick chilling on ice, RNase T1 was added to a final concentration of 500 units/mL and aliquots were taken after 1, 2, and 4 min of incubation at room temperature.

Temperature-Gradient Gel Electrophoresis (TGGE). TGGE was carried out on a commercially available instrument (Qiagen TGGE System). Gels contained 8% (w/v) polyacrylamide (19/1 acrylamide/bisacrylamide), 0.1 \times TBE, 0.1% TEMED, and 0.6% ammonium peroxodisulfate for starting polymerization. The radioactively labeled RNA sample was applied to the broad sample slot in a loading buffer containing 0.1 \times TBE, 4% glycerol, 0.05% xylene cyanol, and 0.025% bromophenol blue. Samples of α Y69 were denatured by boiling in a 95% formamide buffer and were applied to the small slots on either side. For migration of the RNA into the gel matrix, the gel was run for 10 min at 300 V at a uniform temperature of 10 °C. Electrophoresis was then paused for 45 min for equilibration of the 20–70 °C temperature gradient and continued for 1 h at 300 V. Gels were dried and exposed to X-ray film.

Enzymatic Probing of RNA. RNase treatment of the 5'-end-labeled RNA α Y69 (RNase T1, 5' as well as 3'), α Y30, α Y9_{mod}, and asl-1 was performed in hybridization buffer as follows: RNase T1 (Boehringer) for 1–10 min at 20 °C with a 200 units/mL final concentration for all RNA, RNase CI-3 (Boehringer) for 1–8 min at 20 °C (α Y9_{mod}) and 37 °C (α Y69) with a 0.1 unit/mL final concentration in a 10 mM potassium phosphate buffer (pH 6.5) containing 10 mM MgCl₂, RNase Bc (37 °C, 30 units/mL, Pharmacia), RNase A (1–10 min, 37 °C, 10⁻³ unit/mL, Boehringer), and RNase V1 (Pharmacia) at 20 °C for 5 min of incubation with 1, 5, and 10 units/mL (α Y69) and additionally 20 units/mL for α Y30. Aliquots from the reaction mixtures were withdrawn at certain time points, and reactions were stopped by adding the 3-fold volume of stop buffer [8 M urea, 50 mM Tris/HCl (pH 7.6), 15 mM EDTA, 0.2% SDS, 0.04% bromophenol blue, and 0.04% xylene cyanol] or by phenol chloroform extraction followed by ethanol precipitation (RNase V1 reactions). Enzymatic probing of unlabeled SR6 RNA was performed on 10 pmol of RNA for 1, 2, and 4 min at 20 °C with 100 units/mL RNase T1 and 0.1 unit/mL RNase V1.

Cleavages were detected by the reverse transcription method (see below).

Chemical Probing of RNA. Probing reactions were performed with lead(II) acetate and CMCT (Merck), DMS (Aldrich), and kethoxal (U.S. Biochemicals) according to Ehresmann *et al.* (1987). Chemical probing was performed either on 5'-end-labeled α Y69 RNA (50 000 cpm per reaction) or on unlabeled α Y69 or SR6 RNA (10 pmol). For each reaction, a control was treated in parallel, omitting the chemical reagent. After the modification, reactions were stopped by ethanol precipitation in the presence of 0.1 M sodium acetate (pH 6.0).

(a) **Lead-Induced Cleavage.** 5'-Labeled α Y69 RNA, supplemented with 5 μ g of total tRNA, was incubated for 15 min in 20 mM HEPES (pH 7.1), 10 mM magnesium acetate, and 100 mM potassium acetate in the presence of 8 or 16 mM lead acetate. Reactions were stopped by adding 5 μ L of 0.1 M EDTA.

(b) **CMCT Modification.** Unlabeled RNA was incubated in 100 mM NaCl, 10 mM $MgCl_2$, and 50 mM sodium borate at pH 8.0 (native conditions) or in 50 mM sodium borate and 10 mM EDTA at pH 8.0 (semidenaturing conditions) in the presence of 4 μ L of CMCT (40 mg/mL) for 20 min at room temperature.

(c) **Kethoxal Modification.** Unlabeled RNA was modified in hybridization buffer (native conditions) for 10 min or in a buffer containing 20 mM Tris/HCl and 1 mM EDTA at pH 7.4 (semidenaturing conditions) for 5 min in the presence of 2 and 4 μ L of kethoxal (20 mg/mL in 20% ethanol). At the end of each incubation, 20 μ L of 0.05 M potassium borate (pH 7.0) was added for stabilization of the kethoxal–guanosine adduct.

(d) **DMS Modification.** SR6 RNA was modified in hybridization buffer for 6 min at 20 °C with 0.5, 1, and 2 μ L of DMS (diluted 1/8 in ethanol).

Detection and Identification of Cleavages and Modified Nucleotides. Cleavage products derived from reactions carried out on end-labeled RNA were size fractionated on denaturing 12 and 15% polyacrylamide gels. Cleavage positions were identified by running in parallel RNase T1 cleavage products and alkaline hydrolysis products of α Y69, α Y30, α Y9_{mod}, or asl-1, respectively. For detection of modifications induced on unlabeled RNA, the reverse transcription method was used as described by Brunel *et al.* (1991) using a 5'-end-labeled 18mer oligodeoxyribonucleotide complementary to positions 52–69 of α Y69 or to positions 297–309 of SR6. For identification of positions, sequencing lanes were run in parallel.

Alkaline Hydrolysis of Antisense RNA. Pools of successively 3'- or 5'-shortened antisense RNA with identical 5'- or 3'-ends were generated by alkaline hydrolysis of the ³²P-end-labeled RNA α Y69 as described (Rittner *et al.*, 1993; Beijer *et al.*, 1990).

In Vitro Selection Method of Fast-Hybridizing Antisense RNA Species. The experimental procedure was described recently (Rittner *et al.*, 1993; Kronenwett *et al.*, 1996). Briefly, 5'- or 3'-labeled hydrolyzed RNA was incubated with SR6 target RNA (50 or 100 nM final concentration), respectively, in a final volume of 25 μ L of hybridization buffer. At different time points of incubation, 3 μ L aliquots were transferred into 30 μ L of stop buffer precooled on ice. Single-stranded antisense RNA and complexes formed between antisense RNA and target RNA were separated by native agarose gel electrophoresis [1.2%, 89 mM Tris/HCl

(pH 8.3), 89 mM boric acid, and 2 mM EDTA]. Gel slices containing the respective bands were excised and frozen in liquid nitrogen. The RNA was recovered by centrifugation. After precipitation with ethanol, the RNA was redissolved in stop buffer and analyzed by polyacrylamide gel electrophoresis under denaturing conditions (12% polyacrylamide gels containing 7 M urea in 89 mM Tris-borate buffer at pH 8.3). Gels were dried and exposed to X-ray film.

Determination of Association Rate Constants of Antisense RNA. Association rate constants (k_{ass}) were measured as described (Homann *et al.*, 1993). Briefly, radioactively labeled antisense RNA (1 nM final concentration) was incubated with the target RNA SR6 (25, 50, 100, or 200 nM final concentration) in a total volume of 30 μ L of hybridization buffer at 37 °C. After different incubation times, 3 μ L aliquots were withdrawn, transferred into 25 μ L of precooled stop buffer, and analyzed by native polyacrylamide gel electrophoresis. Gels were dried and exposed to X-ray film, and band intensities were determined using a Molecular Dynamics PhosphorImager.

The value of k_{ass} was also calculated from the values of K_D and k_{diss} of the annealing of α Y9_{mod} and SR6. For determination of the K_D value of α Y9_{mod}, 5'-end-labeled antisense RNA (1 nM) was hybridized to unlabeled target RNA SR6 (30, 100, 300, and 1000 nM final concentration) for 6–12 h at 20 and 37 °C in buffer containing 20 mM Tris (pH 7.4), 100 mM NaCl, 10 mM $MgCl_2$, 3% glycerol, and 0.05% xylene cyanol [adapted from Pyle *et al.*, (1990)]. Samples were loaded immediately on running nondenaturing 10% polyacrylamide gels. The dissociation rate constant was measured by adding an excess (600 nM) of unlabeled α Y9_{mod} to preformed double strands between α Y9_{mod} and SR6 (30, 100 and 300 nM SR6) in the buffer described above. Reaction mixtures were incubated at 37 °C. Samples of the reaction mixtures were taken at different time points and were loaded immediately on running nondenaturing 10% polyacrylamide gels. Quantification of band intensities was performed as described above.

RESULTS

The RNA α Y69 Adopts a Defined Conformation. Calculation of lowest-energy secondary structures for α Y69 by the program mfold (Devereux *et al.*, 1984) resulted in two feasible structures that were equally compatible with preliminary probing data (Homann *et al.*, 1993): a double-rod and a Y-shaped structure (Figure 1A). These two structure models are similar in energy [$\Delta G(\text{double-rod}) = -21.6$ kcal/mol and $\Delta G(Y) = -20.7$ kcal/mol] and almost identical in the distribution of double- and single-stranded regions. Due to their different global structure, it is likely that these two conformers are distinguishable by their migration behavior under nondenaturing conditions or by TGGE analysis (Riesner *et al.*, 1991; Rosenbaum *et al.*, 1993; LeCuyer & Crothers, 1993). After purification of *in vitro*-transcribed α Y69, including a step of denaturation and renaturation, this RNA migrates as a single band on a nondenaturing gel, indicating that only one isomer is present in solution (Figure 1B, lane 1). Conversely, additional bands with retarded migration behavior can occasionally be observed directly after *in vitro* transcription, one of which was identified as a dimer of α Y69 (S. Eckardt, unpublished). Purified RNA preparations used for structural probing and for kinetic analyses reproducibly contain only one isoform of α Y69.

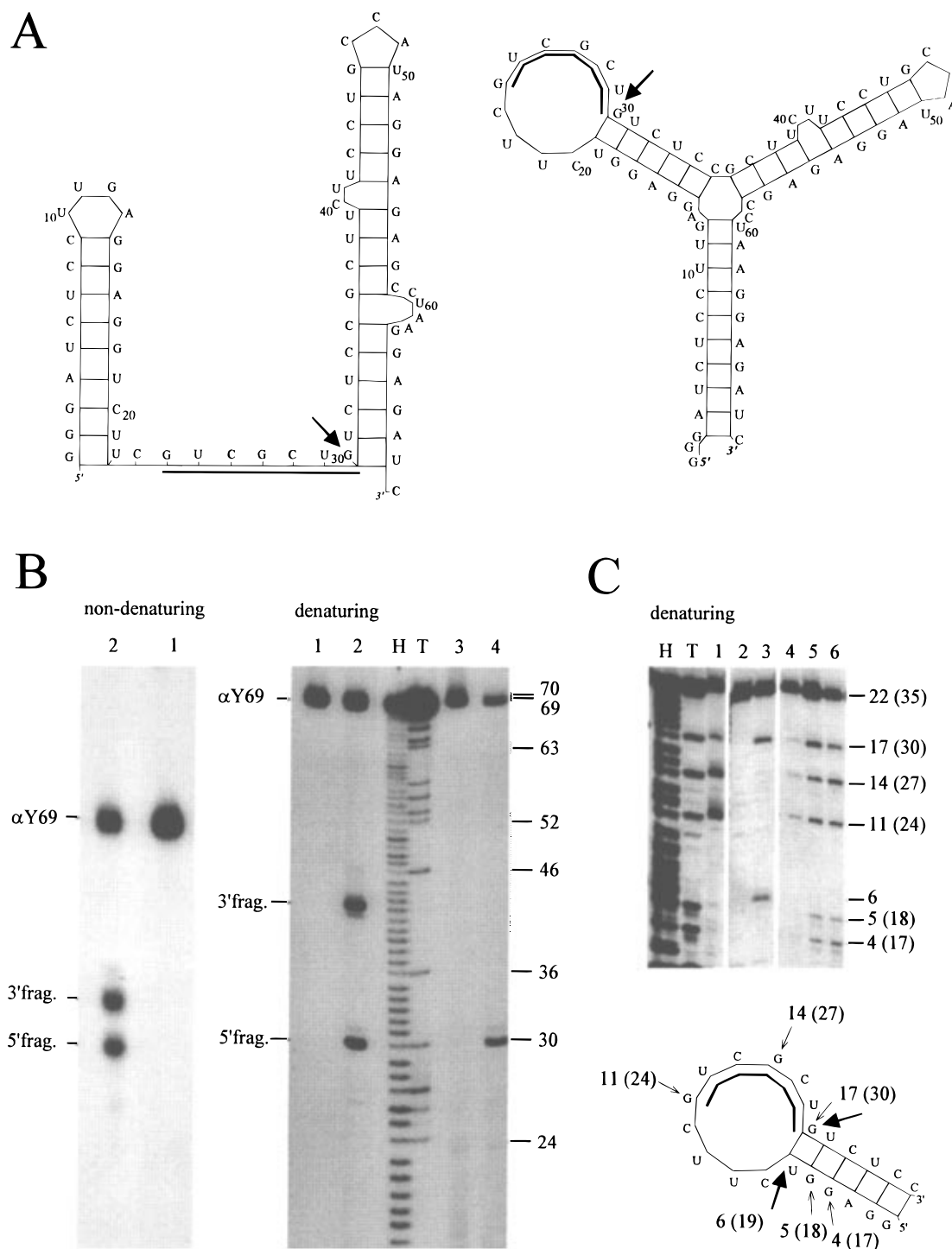


FIGURE 1: (A) Computer-predicted secondary structures of $\alpha Y69$. (B) RNase H cleavage of $\alpha Y69$ induced by a complementary 7mer oligodeoxyribonucleotide (bars in Figure 1A): left, nondenaturing (left panel); right, denaturing 10% polyacrylamide gel; lane 1, untreated uniformly labeled $\alpha Y69$; lane 2, RNase H cleavage reaction of 1; lanes 3 and 4, same as lanes 1 and 2 with 5'-end-labeled RNA; H, alkaline hydrolysis products of 5'-labeled $\alpha Y69$ RNA; T, RNase T1 cleavage of $\alpha Y69$ under denaturing conditions. (C) RNase H cleavage of the synthetic oligoribonucleotide asl-1. Upper panel: denaturing gel analysis of RNase H and T1 cleavages of 5'-end-labeled asl-1; H, alkaline hydrolysis products of 5'-labeled asl-1 RNA; T, T1 cleavage of asl-1 under denaturing conditions; lane 1, limited RNase T1 cleavage; lane 2, untreated incubation control; lane 3, RNase H cleavage products; lane 4, RNase T1 cleavage of nondenatured RNase H cleavage products; lanes 5 and 6, RNase T1 cleavage of denatured RNase H cleavage products (1 and 2 min). Lower panel: proposed secondary structure of asl-1 with indications of RNase T1 (small arrows) and RNase H (large arrows) cleavage sites. Numbers in brackets indicate the respective positions in RNA $\alpha Y69$.

Identification of the Double-Rod Conformer by RNase H Probing. The accessibility of a single-stranded portion in an RNA can be probed by annealing of a complementary oligodeoxyribonucleotide to the respective region and subsequent cleavage of the RNA–DNA hybrid by RNase H (Donis-Keller, 1979; Öhman & Wagner, 1989). To test the

overall conformation of $\alpha Y69$, RNase H cleavage was induced between residues 22 and 30. This stretch of unpaired bases is contained in both alternative structures in a completely different structural context (Figure 1A). Annealing of a complementary 7mer oligodeoxyribonucleotide to $\alpha Y69$ and subsequent RNase H cleavage result in release

of two fragments under nondenaturing conditions (Figure 1B, left panel, lane 2). Identification of the cleavage products by denaturing gel electrophoresis shows that RNase H cleavage occurs 3' with respect to position 30 of α Y69 at the end of the RNA–DNA hybrid, followed by further exonucleolytic cleavage of the RNA strand (Figure 1B, right panel, lane 2). A comparison of cleavage products generated from uniformly labeled and 5'-end-labeled α Y69 on both nondenaturing (data not shown) and denaturing gel electrophoresis shows that the fragment with the higher electrophoretic mobility on a nondenaturing gel carries the 5'-label and corresponds to the 30 upstream nucleotides of α Y69 and the slower-migrating one to the 3'-portion (Figure 1B, right panel, lanes 2 and 4). The 5'-cleavage product migrates similarly with respect to the synthetic oligoribonucleotide α Y30 of the same sequence (see Material and Methods) on a nondenaturing gel (data not shown). Because of the different base composition, the 3'-fragment of 39 bases shows retarded migration behavior and comigrates with the 5'-labeled 42mer. Due to run-off *in vitro* transcription by T7 RNA polymerase from a linearized plasmid template, the RNA preparation contains a 69mer and 70mer (see lane 4). As visualized by probing of end-labeled RNA, these RNA differ by one nucleotide at the 3'-end and therefore do not represent different populations.

To investigate whether release of the two fragments under nondenaturing conditions (Figure 1B, left panel) indicates the double-rod conformer or whether it could be due to melting of the Y structure during cleavage, the synthetic oligoribonucleotide asl-1 (residues 15–36 of α Y69, including the target site for the complementary oligodeoxyribonucleotide) was used as a control target. This molecule represents the large loop of the Y structure with a six-base-pair stem and folds into the predicted structure as verified by RNase T1 probing (Figure 1C, lane 1; only G residues in the loop are accessible to cleavage under limiting conditions). RNase H cleavage results in a 17mer product due to cleavage at the 3'-end of the RNA–DNA duplex (Figure 1C, lane 3). Additionally, cleavage products of six and five bases were observed in different experiments, which might be due to cleavage on the opposite side of the helical stem. In the nondenatured cleavage product, G residues 4 and 5 of the helical stem remain protected with respect to RNase T1 cleavage, indicating that the six-base pair stem does not melt under cleavage conditions (Figure 1C, lane 4). After heat denaturation of the sample, the same residues become accessible for RNase T1 (Figure 1C, lanes 5 and 6). Due to hybridization of the complementary 7mer oligodeoxyribonucleotide to residues 11–17 of asl-1, the three RNase T1 sensitive sites in the loop (positions 11, 14, and 17, Figure 1C, lane 1) are partially protected. Further, analysis of RNase H cleavage products of asl-1 by nondenaturing gel electrophoresis revealed two products, a fast-migrating smaller fragment corresponding to the minor product of six bases and the full length molecule.

These results provide strong evidence for the double-rod model. In this conformation, the target region for RNase H cleavage represents a hinge part between two stem–loop elements. Cleavage results in release of these two elements. In the alternative Y-like structure, the cleavage site is located at the 3'-end of the large loop. Release of two cleavage products from this structure would only be possible after complete denaturation of the molecule.

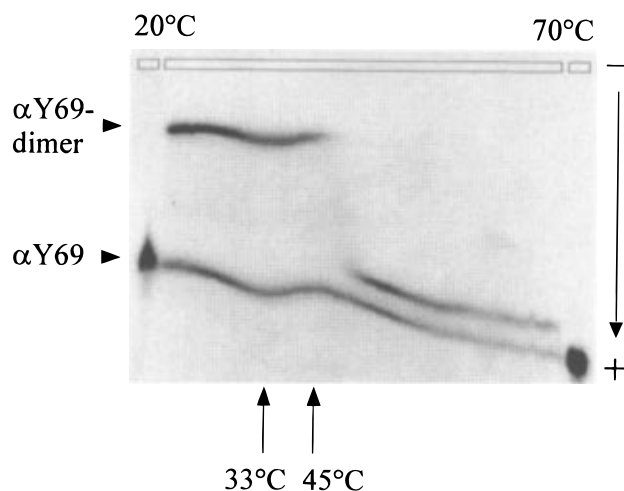


FIGURE 2: Temperature gel electrophoresis of monomeric and dimeric forms of α Y69 (broad central slot). Formamide-denatured 5'-end-labeled α Y69 was applied to the left and right small slots.

Temperature-Gradient Gel Electrophoresis of α Y69. A renatured α Y69 RNA preparation containing the dimer was analyzed by temperature-gradient gel electrophoresis. The monomer migrates as a single band with two transitions at 33 and 45 °C (Figure 2). The two transitions are consistent with the melting of the two stem–loop elements of the double-rod conformer. Heterodimer analyses with shortened derivatives of α Y69 suggest that the dimer is formed via sequences of the 5'-stem–loop (data not shown). Thus, the thermal transition of the monomer and the dimer at 45 °C indicates the cooperative melting of the dimer as well as melting of the 5'-stem–loop of α Y69 (Figure 2).

Enzymatic Secondary Structure Probing of α Y69. The secondary structure of α Y69 RNA was further analyzed using enzymatic and chemical probing methods (Ehresmann *et al.*, 1987). Limited cleavage by single-strand-specific ribonucleases and identification of susceptible sites allow mapping of nonpaired bases within an RNA. The RNA α Y69 was probed using ribonucleases T1, Cl-3, Bc, and A. Additionally, ribonuclease V1 cleavage reactions were performed to indicate regions with a double-helical or stacked conformation (Auron *et al.*, 1982; Lowman & Draper, 1986). Cleavage patterns are shown in the upper panel of Figure 3 (left, single-strand-specific RNases; middle, RNase V1); the lower panel (left) summarizes the compatibility of cleavage sites with the proposed secondary structure model. Both loops of the two stem–loop elements are susceptible to cleavage by RNase T1, Bc, or A. The presumed hinge region represents a major target for all single-strand-specific ribonucleases used, whereas the two helical stems show an overall protection. An exception to this is RNase Bc cleavage at the end of the 5'-stem–loop (positions 19 and 20). RNase V1 cleavage is restricted primarily to double-stranded portions of α Y69. However, cleavages also occur in the 5'-end of the single-stranded hinge, indicating a possible stacked conformation.

Chemical Probing of α Y69. Chemical probing reagents are smaller in size than enzymes and modify specific atomic positions of bases or phosphates in RNA. Two base-specific reagents were used: CMCT which reacts with uridine at N3 and to a lesser extent with guanine at N1 (Figure 3, upper right panel) and kethoxal which modifies guanine at the N1 and N2 positions. Additionally, α Y69 was cleaved with lead acetate (Figure 3, upper middle panel), which has a prefer-

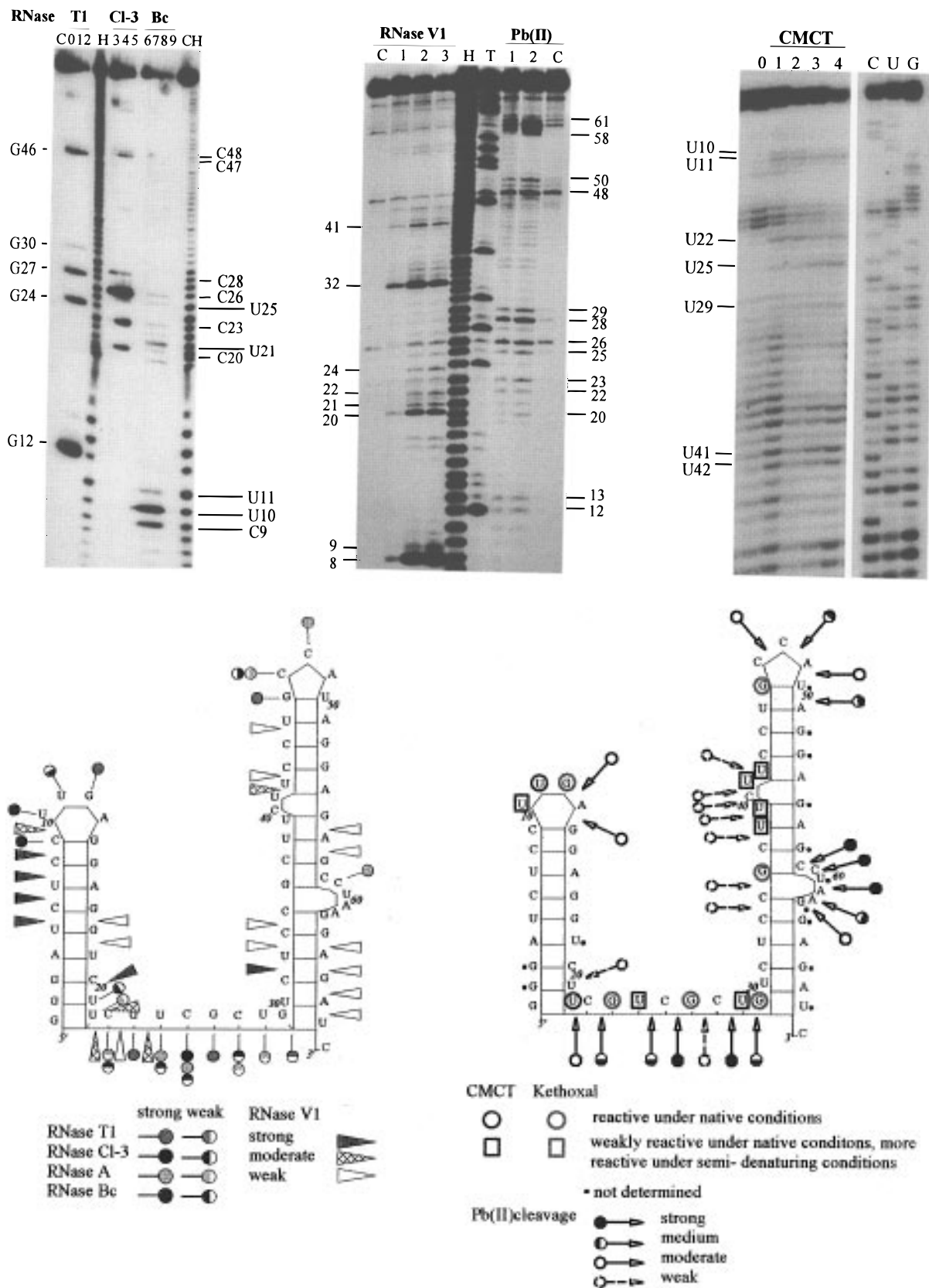


FIGURE 3: Enzymatic and chemical probing of $\alpha Y69$. (Upper left panel) Probing with RNase T1 (2, 4, and 8 min), RNase CI-3 (0.5, 2, and 5 min), and RNase Bc (0.5, 1, 2, 4, and 8 min) (see Materials and Methods): C, incubation control; H, alkaline hydrolysis products; T, T1 cleavage of $\alpha Y69$ under denaturing conditions. (Upper center panel) RNase V1 hydrolysis and chemical probing with Pb(II) acetate (see Materials and Methods). Major cleavage sites are indicated. Lanes H, T, and C are as above. (Upper right panel) CMCT probing of $\alpha Y69$: lanes 0, incubation control; lanes 1–2, native conditions; lanes 3–4, semidenaturing conditions (see Materials and Methods); C, U, and G, $\alpha Y69$ RNA sequencing lanes. (Lower panels) Summary of enzymatic (left) and chemical (right) probing data. Only major cuts are indicated. The absence of symbols in the right panel indicates no reactivity for G and U residues. Reactivities of C and A residues were not determined.

ential affinity for single-stranded regions or weakly stable helices within an RNA (Gornicki *et al.*, 1989). The results

of the chemical probing are summarized on the secondary structure of $\alpha Y69$ in the lower right panel of Figure 3. Lead

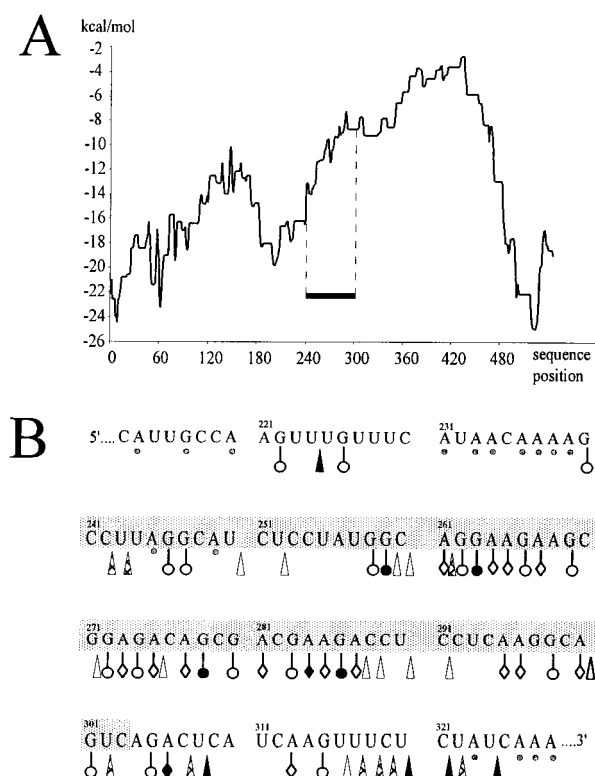


FIGURE 4: (A) Calculated minimum energies (folding potential) of 100-nucleotide segments of the HIV-1-derived target sequence. The bar indicates the sequence complementary to α Y69. (B) Secondary structure probing of the subregion of SR6 complementary to α Y69 (shaded portion). Probing was performed with RNase T1 (circles), RNase V1 (arrowheads), and DMS (rhomboid symbols) (see Materials and Methods). Filled symbols denote strong reactivity; hatched and empty symbols moderate and weak reactivity, respectively. Small circles denote not determined; no symbol denotes the absence of reactivity for C and G positions. Reactivities of A and U residues were not determined.

acetate-induced cleavage of α Y69 is mainly observed in portions proposed to be single-stranded. Major targets for cleavage are found in the hinge region with strong cleavages at positions 26 and 28 and in the large bulge (positions 58–62) of the 3'-stem-loop. Similarly, reactivity of U residues toward modification by CMCT can only be observed in single-stranded parts of the secondary structure model and not in the predicted helical stems. Under semidenaturing conditions, the weak reactivities of U10 in the 5'-stem-loop and of U38, U 39, U41, and U42 in a bulged portion of the 3'-stem-loop are increased, indicating alternative base pairing and breathing of base pairs in these regions.

Probing of G residues by kethoxal modification resulted in essentially the same reactivity pattern as observed in RNase T1 cleavage. One additional reactive site at position G36 was detected.

Structures of the Target RNA SR6. The predicted structure of the 645-nucleotide HIV-1 *tat/rev*-derived target RNA SR6 is characterized by a high free energy [Figure 4A and Sczakiel *et al.* (1993)] indicating a low degree of secondary structure formation. Calculations of lowest-energy structures for SR6 by the computer program *mfold* result in a large number of different structures with similar ΔG values (between -127.1 and -121.0 kcal/mol for the 10 lowest-energy structures with *mfold* 2.0).

Chemical and enzymatic probing of the complete SR6 RNA showed a high overall reactivity to single-strand-specific reagents in the region complementary to α Y69 (Figure

4B) which is consistent with the low folding potential. An equilibrium of closely related structures of SR6 could coexist in solution. Due to the great number of possible conformers that are similar in free energy and the compatibility of the probing data with more than one structure, a defined secondary structure model for SR6 cannot be derived.

Kinetic Mapping of α Y69. Two separate pools of successively 3'- or 5'-shortened derivatives of end-labeled α Y69 were generated by limited alkaline hydrolysis of 5'- or 3'- 32 P-labeled α Y69. By an *in vitro* selection (see Materials and Methods), the relative annealing rate of each antisense species of the pools to SR6 was monitored. The distribution and chain length of single-stranded and hybridized fractions were analyzed at certain time points of the reactions. For 3'-end-labeled, successively 5'-shortened derivatives of α Y69, fast association with the target RNA SR6 can only be detected for species that contain C26 or upstream sequences (Figure 5A). Smaller species that contain only sequences downstream of C28 hybridize substantially slower. For the pool of 3'-shortened derivatives, there is no measurable annealing in the time window of the experiment (16 min) for RNA shorter than 26 bases. Maximal annealing that is comparable to that of α Y69 is achieved at a minimal length of 28 nucleotides (Figure 5B). The threshold length of 28 nucleotides was not due to instability of the duplex under the experimental conditions (unpublished).

Kinetic and Structural Analysis of Elements of α Y69. To investigate the role of individual structural elements of α Y69, including the hinge sequence for the annealing to SR6, association kinetics of several α Y69-derived modified RNAs were investigated. Secondary structure models of the shortened (α Y30 and *asl-1*) or modified (α Y9_{mod}) derivatives of α Y69 were calculated by *mfold* and verified by enzymatic probing of 5'-end-labeled RNA (Figure 6). The oligoribonucleotide α Y30 represents an α Y69 molecule truncated at position 30. The predicted secondary structure is identical to the 5'-portion of α Y69, including the 5'-stem-loop and the single-stranded hinge. This structure was confirmed by RNase T1 and V1 digestions (Figure 6). Cleavage sites and intensities were identical to the ones observed in α Y69 (RNase T1) or consistent with the structure (RNase V1). The oligoribonucleotide α Y9_{mod} was designed to fold into a structure similar to α Y69. This RNA contains the single-stranded hinge region of α Y69 flanked by two noncomplementary and shorter 5'- and 3'-stem-loops (see Material and Methods and Figure 6). Accessibilities of the hinge nucleotides to the single-strand-specific RNases T1 and Cl-3 were almost identical as in α Y69. The G and C residues in the predicted stems were not sensitive to cleavage by single-strand-specific RNases (Figure 6) except for position 33 (RNase Cl-3). The oligoribonucleotide *asl-1* contains residues 14–35 of α Y69 and is proposed to form a large loop that contains the hinge portion of the double rod (positions 23–29) and three more 5'-residues, flanked by a six-base pair stem. Limited digestion with RNase T1 resulted in the three cleavage sites in the loop portion, whereas G residues of the stems were not accessible for the enzyme (Figure 6).

Association rate constants were determined for all RNAs using SR6 as a target. The k_{ass} values for α Y30 and α Y9_{mod} were 6×10^4 and $1 \times 10^3 \text{ M}^{-1} \text{ s}^{-1}$, respectively (Figure 7). Association rate constants for α Y69-derived mutants α Y69-mut1 ($0.5 \times 10^4 \text{ M}^{-1} \text{ s}^{-1}$) and α Y69-mut6 ($3.0 \times 10^4 \text{ M}^{-1} \text{ s}^{-1}$) had been determined previously (Homann *et al.*, 1993).

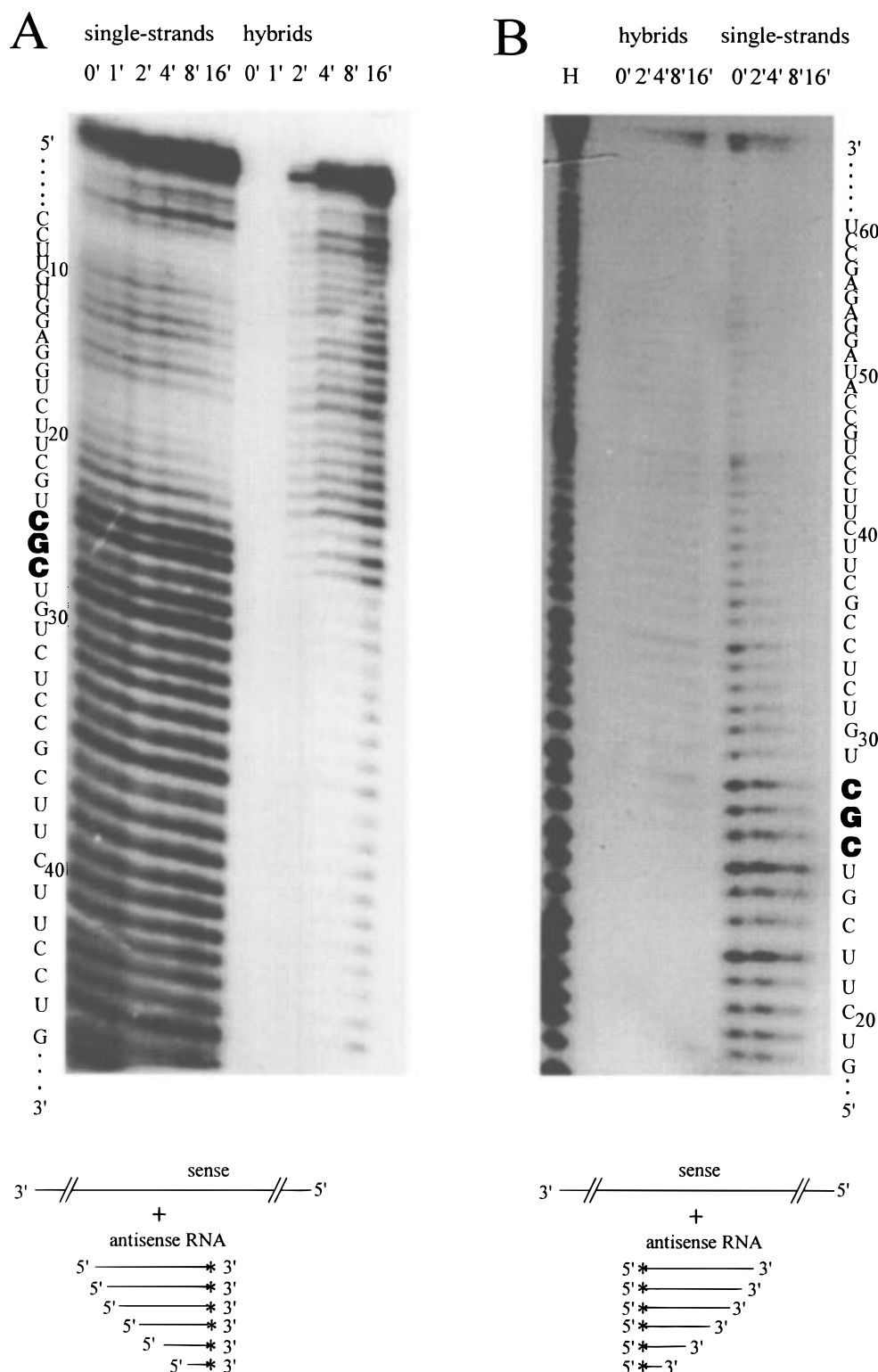


FIGURE 5: Kinetic mapping of $\alpha Y69$. The annealing reactions between 3'- or 5'-truncated derivatives of $\alpha Y69$ and SR6 are analyzed at the time points indicated on top (minutes). Analysis of the composition and chain length of single-stranded and hybrid fractions by denaturing gel electrophoresis. Bold letters in the sequence of $\alpha Y69$ denote positions 26–28 required for fast annealing. Asterisks in the reaction schemes below indicate the radioactively labeled 5'-ends of $\alpha Y69$ derivatives: (A) 5'-truncated $\alpha Y69$ and (B), 3'-truncated $\alpha Y69$.

Base pairing between $\alpha Y9_{\text{mod}}$ (Figure 6) and SR6 is limited to a stretch of only nine complementary bases. Formation of a double strand could be detected on nondenaturing gels. The stability of this duplex was dependent on the presence of Mg^{2+} ions. Therefore, all gel shift analyses were carried out on nondenaturing 10% polyacrylamide gels in the presence of 10 mM MgCl_2 in gels and running buffer. Comparison of RNase T1 digestions of single-stranded 5'-end-labeled $\alpha Y9_{\text{mod}}$ RNA and the duplex showed protection

of cleavage sites contained in the single-stranded hinge portion. Two sites in the noncomplementary stem-loops became accessible (data not shown). This indicates that the detected duplex is due to base pairing between the molecules. As the RNA are associated only via nine base pairs, one could assume that duplex formation is not irreversible as is the case for long chain duplex RNA (Homann *et al.*, 1996). For this reason, we also measured the K_D value and dissociation rate constant for $\alpha Y9_{\text{mod}}$ and SR6 and calculated

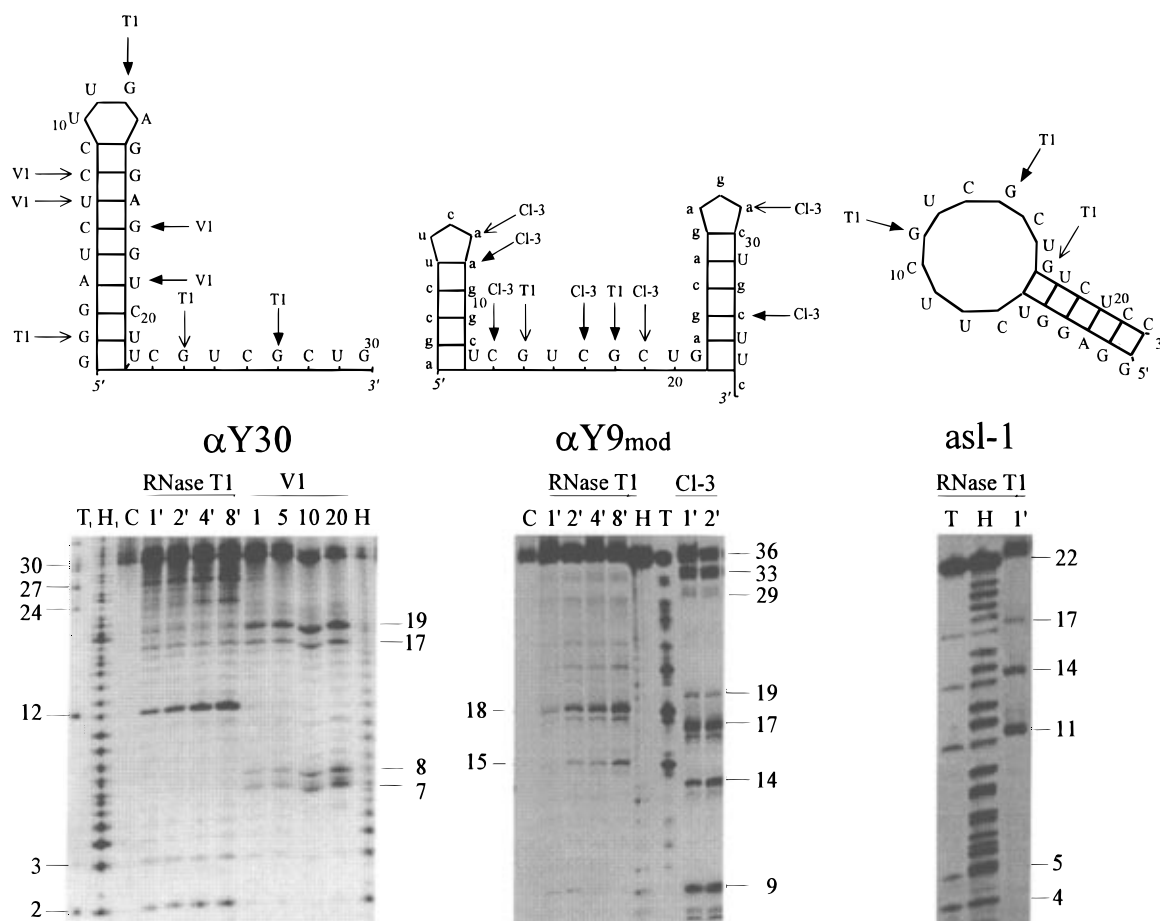


FIGURE 6: (Upper panels) Secondary structure models for derivatives of $\alpha Y69$ based on mfold calculations. Cleavage sites for single- and double-stranded specific RNases are marked with arrows (filled arrowhead, strong; plain arrow, moderate). Capital letters in the sequence of $\alpha Y9_{mod}$ indicate bases complementary to SR6. (Lower panels) Enzymatic probing of derivatives. Enzymes and time courses (minutes) are indicated on top (RNase V1, units per milliliter final concentration) (see Materials and Methods). Positions of major cleavage sites are indicated: C, incubation control; H, alkaline hydrolysis products of each RNA as size marker; T, T1 cleavage of RNA under denaturing conditions. T₁ and H₁ are products of 5'-end-labeled RNA $\alpha Y69$.

the value for k_{ass} which was compatible with the value determined from initial annealing rates ($1 \times 10^3 \text{ M}^{-1} \text{ s}^{-1}$, Figure 7).

A second set of $\alpha Y69$ derivatives was generated by introducing three base exchanges in the single-stranded hinge region of $\alpha Y69$ (positions 26–28). This CGC triplet was required for fast annealing of both of 3'- and 5'-truncated derivatives (see Figure 5). For further studies, five derivatives were chosen for which the two lowest-energy secondary structures were identical with those for the wild type molecule. The five derivatives $\alpha Y69$ -1–5 showed a migration behavior on nondenaturing acrylamide gels that did not distinguish it from $\alpha Y69$, indicating a similar overall structure. Enzymatic secondary structure probing using RNase T1 and RNase CI-3 is consistent with the double-rod structure (data not shown). Annealing reactions of the derivatives with SR6 followed second-order kinetics. The 10-fold-decreased association rate constants for the annealing of the derivatives of $\alpha Y69$ with SR6 *in vitro* demonstrate the importance of the CGC triplet for fast annealing (Table 1). Similarly, mismatches at positions 278–280 of SR6 that are complementary to positions 26–28 of $\alpha Y69$ reduced k_{ass} by the same factor. An exchange of the critical GCG triplet of SR6 with a CGC (SR6-5) which retains the total number of GC base pairs in the duplex $\alpha Y69$ -5/SR6-5 restored the full annealing rate (Table 1).

DISCUSSION

Of two secondary structure models with different global structures but similar of paired and unpaired portions, only one conformer is obtained in purified α Y69 RNA and is obvious from nondenaturing gel analysis (Figure 1). Cleavage experiments with RNase H led to the release of two fragments under nondenaturing conditions. This strongly supports the two-element structure of the double-rod model. Incomplete cleavage by the enzyme does not indicate a second conformer hidden in the uncleaved portion. Most likely, inefficient cleavage is due to the suboptimal reaction conditions used in the assay concerning temperature as well as length and positioning of the complementary oligodeoxyribonucleotide. Incomplete RNase H cleavage has been reported elsewhere (Duroux *et al.*, 1995; Crooke *et al.*, 1995). Further, analysis of RNA preparations by TGGE excludes coexisting structures and provides strong evidence for the double-rod conformer of α Y69 (Figure 2).

Enzymatic and chemical probing data confirm this double-rod model of $\alpha Y69$ and provide more detailed information on its structure. The two stem-loop elements are connected via a highly accessible and single-stranded hinge region. Increased flexibility in the 3'-portion of the hinge is indicated by pronounced cleavages by lead(II) acetate in this portion (see Figure 3). Some of the bases in the 5'-part of the hinge might adopt a stacked conformation as reflected in the

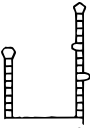
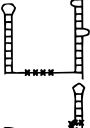
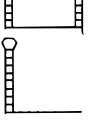

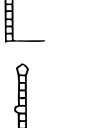
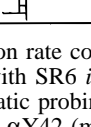
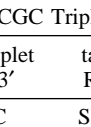
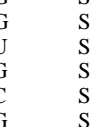
RNA	secondary structure	k_{ass} ($\text{M}^{-1} \text{s}^{-1}$)
αY69		2.9×10^4
$\alpha\text{Y69-mut1}$		5.0×10^3
$\alpha\text{Y69-mut6}$		3.0×10^4
αY30		6.0×10^4
αY9mod		1.0×10^3
asl-1		7.0×10^4
αY26		$\ll 10^3$
αY42		$\ll 10^3$

FIGURE 7: Association rate constants for annealing of αY69 and derivatives thereof with SR6 *in vitro*. Secondary structures were confirmed by enzymatic probing [this work and Homann (1995)] except for αY26 and αY42 (mfold calculations).

Table 1: Role of the CGC Triplet of αY69 for Annealing

antisense RNA	base triplet 5'→3'	target RNA	base triplet 5'→3'	k_{ass} ($\text{M}^{-1} \text{s}^{-1}$) ^a
αY69	CGC	SR6	GCG	2.9×10^4
$\alpha\text{Y69-1}$	AUA	SR6	GCG	2.5×10^3
$\alpha\text{Y69-2}$	AUG	SR6	GCG	2.9×10^3
$\alpha\text{Y69-3}$	GUG	SR6	GCG	3.2×10^3
$\alpha\text{Y69-4}$	ACU	SR6	GCG	2.3×10^3
$\alpha\text{Y69-5}$	GCG	SR6	GCG	4.2×10^3
αY69	CGC	SR6-5	CGC	4.1×10^3
$\alpha\text{Y69-5}$	GCG	SR6-5	CGC	3.0×10^4

^a Standard deviation of 10–40%.

reactivity with respect to RNase V1. The 5'-stem-loop element is confirmed by strong RNase V1 cleavages on either end of the nine-base pair helix and substantial susceptibility of the four loop bases to single-strand specific probes. In the lower part of the stem, RNase Bc, RNase A, and lead acetate cleavage (positions 20–22) and reactivity of U22 with respect to CMCT suggest breathing of the last two base pairs of the helix. However, in RNase T1 cleavage experiments on both 5'- and 3'-end-labeled αY69 , G residues

(positions 1–3) in this portion are only weakly accessible to the enzyme (data not shown) suggesting some degree of base pairing. The less stable helix of the 3'-stem-loop is interrupted by two areas with bulged-out nucleotides. In the upper bulge, weak reactivities obtained in CMCT and lead acetate probing could indicate alternative base pairings between A56 and U38/U39 and A54 and U41/U42. Similarly, a base pair between C40 and G55 could be formed.

Structural and kinetic investigations on the HIV-directed antisense RNA αY69 and its target provide evidence for a distinct annealing mechanism. Kinetic mapping data suggest that the unpaired hinge of αY69 including a sequence of three bases located in its 3'-part (positions 26–28, see Figure 2), is necessary for fast hybridization. Disruption of complementarity between αY69 and SR6 at the three positions (26–28 of αY69 and 278–280 of SR6) leads to a 10-fold-decreased annealing (Table 1). An exchange of a total of four bases including two of the three bases (26 and 27), reduces k_{ass} significantly but in a less pronounced manner (factor of 6; $\alpha\text{Y69-mut1}$, Figure 7), whereas introduction of five mismatches into the 3'-stem-loop element does not alter the association rate constant ($\alpha\text{Y69-mut6}$, Figure 7). Thus, an interaction between the complementary triplets 26–28 and 278–280 seems to be the critical step for the annealing reaction between αY69 and SR6. This is further reflected by the fast annealing of a complementary pair of mutants carrying a reciprocal exchange of this triplet between sense and antisense RNA ($\alpha\text{Y69-5}$ and SR6-5, Table 1).

These data suggest that the 3'- and 5'-stem-loop elements of αY69 are not involved in the rate-limiting step of the annealing reaction. However, an influence of the flanking 5'- and 3'-located stem-loop elements on association kinetics can be observed. Deletion of the 3'-stem-loop element in the construct αY30 significantly increases k_{ass} (k_{ass} for αY30 of $6 \times 10^4 \text{ M}^{-1} \text{s}^{-1}$ and for αY69 of $2.9 \times 10^4 \text{ M}^{-1} \text{s}^{-1}$). In contrast, introduction of noncomplementary stem-loop elements 3' and 5' in αY9mod leads to a drastic reduction of k_{ass} (Figure 7). Fast association is observed for the oligonucleotide asl-1 (k_{ass} of $7 \times 10^4 \text{ M}^{-1} \text{s}^{-1}$). In this αY69 derivative, the hinge sequence is unpaired, though contained in a different structural context. Fast annealing of this RNA is consistent with the observation that the availability of the three hinge bases and the complementarity of the flanking sequences are crucial for fast annealing.

A simple general scheme for the duplex formation between complementary RNA is shown in Figure 8. In a first diffusion-controlled step, both RNAs can form a precomplex that does not involve base-specific interactions. Subsequently, a reversible initial base-specific complex is formed which in some cases is called “kissing” complex (Eguchi & Tomizawa, 1990; Eguchi *et al.*, 1991). Finally, duplex formation is initiated and the duplex elongates to form the complete RNA double strand. Often, both base-specific steps involve RNA sequences at different sites. For αY69 , the data of this work suggest that both base-specific initial interactions and initiation of duplex formation occur at the 3'-portion of the hinge region (positions 26–28). As there are no free ends available in αY69 , initiation of duplex formation is most likely to also proceed from the central

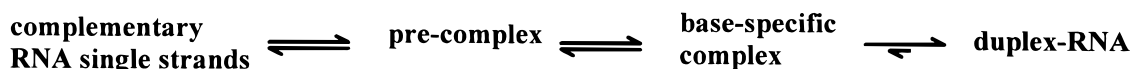


FIGURE 8: Simplified scheme for RNA–RNA annealing.

hinge region. In contrast to several annealing mechanisms known from natural antisense-regulated systems, no interactions between structurally defined stem–loop elements are involved in the initial step of the annealing between α Y69 and SR6. This interaction involving the single-stranded hinge region of α Y69 and an unstructured region of SR6 shares some similarity with the *hok-sok* system of *E. coli* (Thisted *et al.*, 1994). In this system, however, the long unpaired 5'-end of *hok* RNA is required, whereas the part of α Y69 mediating initiation of duplex formation is flanked by two stem–loop elements.

The data of this work are consistent with a “one-site” mechanism of RNA–RNA annealing in which a central and surprisingly unstructured part of an RNA mediates base-specific RNA–RNA interactions. This pathway represents a highly distinctive and alternative pathway of RNA duplex formation.

Fast-annealing pairs of complementary RNA often associate via initial loop–loop interactions (Wagner & Simons, 1994). The relatively slow annealing rates of the *hok-sok* system and α Y69 and SR6 on the order of $3 \times 10^4 \text{ M}^{-1} \text{ s}^{-1}$ could be due to the lack of recognition via stem–loop elements. Still, efficient antisense inhibition is mediated in both systems *in vivo*. Thus, one could speculate that RNA–RNA annealing is increased *in vivo* by cellular factors. This is supported by the finding that the annealing of α Y69 and SR6 is increased by 3 orders of magnitude by a recombinant p53 protein *in vitro* (Nedbal *et al.*, 1997). If this increased annealing also occurs *in vivo*, it would be interesting to identify the structural prerequisites of the RNA for facilitated annealing.

ACKNOWLEDGMENT

We cordially thank G. Steger and E. Westhof for stimulating discussions as well as C. Ehresmann and B. Ehresmann for helpful advice.

REFERENCES

- Auron, P. E., Weber, L. D., & Rich, A. (1982) *Biochemistry* 21, 4700.
- Beijer, B., Sulston, I., Sproat, B. S., Rider, P., Lamond, A. I., & Neuner, P. (1990) *Nucleic Acids Res.* 18, 5143.
- Brunel, C., Romby, P., Westhof, E., Ehresmann, C., & Ehresmann, B. (1991) *J. Mol. Biol.* 221, 293.
- Case, C. C., Roels, S. M., Jensen, P. D., Lee, J., Kleckner, N., & Simons, R. W. (1989) *EMBO J.* 8, 4297.
- Crooke, S. T., Lemonidis, K. M., Neilson, L., Griffey, R., Lesnik, E. A., & Monia, B. P. (1995) *Biochem. J.* 312, 599.
- Devereux, J., Haerberli, P., & Smithies, O. (1984) *Nucleic Acids Res.* 12, 387.
- Donis-Keller, H. (1979) *Nucleic Acids Res.* 7, 179.
- Duroux, I., Godard, G., Boidot Forget, M., Schwab, G., Hélène, C., & Saison Behmoaras, T. (1995) *Nucleic Acids Res.* 23, 3411.
- Eguchi, Y., & Tomizawa, J. (1990) *Cell* 60, 199.
- Eguchi, Y., & Tomizawa, J. (1991) *J. Mol. Biol.* 220, 831.
- Eguchi, Y., Itoh, T., & Tomizawa, J. (1991) *Annu. Rev. Biochem.* 60, 631.
- Ehresmann, C., Baudin, F., Mougél, M., Romby, P., Ebel, J. P., & Ehresmann, B. (1987) *Nucleic Acids Res.* 15, 9109.
- Erickson, R. P., & Izant, J. G., Eds. (1992) *Gene Regulation: Biology of Antisense DNA and RNA*, Raven Press, New York.
- Gornicki, P., Baudin, F., Romby, P., Wiewiorowski, M., Kryzosiak, W., Ebel, J. P., Ehresmann, C., & Ehresmann, B. (1989) *J. Biomol. Struct. Dyn.* 6, 971.
- Hjalt, T., & Wagner, E. G. (1992) *Nucleic Acids Res.* 20, 6723.
- Hjalt, T. A., & Wagner, E. G. (1995) *Nucleic Acids Res.* 23, 571.
- Homann, M. (1995) Ph.D. Thesis, University of Heidelberg, Heidelberg, Germany.
- Homann, M., Rittner, K., & Sczakiel, G. (1993) *J. Mol. Biol.* 233, 7.
- Homann, M., Nedbal, W., & Sczakiel, G. (1996) *Nucleic Acids Res.* 24, 4395.
- Jain, C. (1995) *J. Mol. Biol.* 246, 585.
- Junker, U., Rittner, K., Homann, M., Bevec, D., Bohnlein, E., & Sczakiel, G. (1994) *Antisense Res. Dev.* 4, 165.
- Kittle, J. D., Simons, R. W., Lee, J., & Kleckner, N. (1989) *J. Mol. Biol.* 210, 561.
- Kronenwett, R., Haas, R., & Sczakiel, G. (1996) *J. Mol. Biol.* 259, 632.
- LeCuyer, K., & Crothers, D. M. (1993) *Biochemistry* 32, 5301.
- Lowman, H. B., & Draper, D. E. (1986) *J. Biol. Chem.* 261, 5396.
- Nedbal, W., Frey, M., Willemann, B., Zentgraf, H., & Sczakiel, G. (1997) *J. Mol. Biol.* 266, 677.
- Öhman, M., & Wagner, E. G. (1989) *Nucleic Acids Res.* 17, 2557.
- Persson, C., Wagner, E. G., & Nordstrom, K. (1990) *EMBO J.* 9, 3777.
- Pyle, A. M., Mc Swiggen, J. A., Cech, T. R. (1990) *Proc. Natl. Acad. Sci. U.S.A.* 87, 8187.
- Riesner, D., Henco, C., & Steger, G. (1991) in *Advances in Electrophoresis*, Vol. 4, pp 69–250, VCH, Weinheim, Germany.
- Rittner, K., & Sczakiel, G. (1991) *Nucleic Acids Res.* 19, 1421.
- Rittner, K., Burmester, C., & Sczakiel, G. (1993) *Nucleic Acids Res.* 21, 1381.
- Rosenbaum, V., Klahn, T., Lundberg, U., Holmgren, E., von Gabain, A., & Riesner, D. (1993) *J. Mol. Biol.* 229, 656.
- Sczakiel, G., Homann, M., & Rittner, K. (1993) *Antisense Res. Dev.* 3, 45.
- Senger, M., Glatting, K. H., Ritter, O., & Suhai, S. (1995) *Comput. Methods Programs Biomed.* 46, 131.
- Simons, R. W., & Kleckner, N. (1988) *Annu. Rev. Genet.* 22, 567.
- Thisted, T., Sorensen, N. S., Wagner, E. G., & Gerdes, K. (1994) *EMBO J.* 13, 1960.
- Wagner, E. G., & Simons, R. W. (1994) *Annu. Rev. Microbiol.* 48, 713.

BI9707234